remote sensing

MDPI

Article

Phenology Plays an Important Role in the Regulation of Terrestrial Ecosystem Water-Use Efficiency in the Northern Hemisphere

Jiaxin Jin [1,*], Ying Wang [2], Zhen Zhang [3,4], Vincenzo Magliulo [5], Hong Jiang [1,*] and Min Cheng [1]

1 International Institute for Earth System Science, Nanjing University, Nanjing 210023, China; chengmin007008@163.com
2 Nanjing Institute of Geography & Limnology, Chinese Academy of Sciences, Nanjing 210008, China; mfacewang@gmail.com
3 Dynamic Macroecology, Swiss Federal Research Institute WSL, Zürcherstrasse 111, 8903 Birmensdorf, Switzerland; yuisheng@gmail.com
4 Cold and Arid Regions Environmental and Engineering Research Institute, Chinese Academy of Sciences, Lanzhou 730000, China
5 CNR Institute for Agricultural and Forest Systems, Via Patacca 85, 80056 Ercolano, Italy; enzo.magliulo@cnr.it
* Correspondence: jinjiaxin@nju.edu.cn (J.J.); jh_china2012@hotmail.com (H.J.); Tel.: +86-25-8968-5969 (J.J. & H.J.)

Academic Editor: Clement Atzberger
Received: 2 June 2017; Accepted: 25 June 2017; Published: 28 June 2017

Abstract: Ecosystem-scale water-use efficiency (WUE), defined as the ratio of gross primary productivity (GPP) to evapotranspiration (ET), is an important indicator of coupled carbon-water cycles. Relationships between WUE and environmental factors have been widely investigated, but the variations in WUE in response to biotic factors remain little understood. Here, we argue that phenology plays an important role in the regulation of WUE by analyzing seasonal WUE responses to variability of photosynthetic phenological factors in terrestrial ecosystems of the Northern Hemisphere using MODIS satellite observations during 2000–2014. Our results show that WUE, during spring and autumn is widely and significantly correlated to the start (SOS) and end (EOS) of growing season, respectively, after controlling for environmental factors (including temperature, precipitation, radiation and atmospheric carbon dioxide concentration). The main patterns of WUE response to phenology suggest that an increase in spring (or autumn) WUE with an earlier SOS (or later EOS) are mainly because the increase in GPP is relatively large in magnitude compared to that of ET, or due to an increase in GPP accompanied by a decrease in ET, resulting from an advanced SOS (or a delayed EOS). Our results and conclusions are helpful to complement our knowledge of the biological regulatory mechanisms underlying coupled carbon-water cycles.

Keywords: water-use efficiency; phenology; gross primary product; evapotranspiration; remote sensing

1. Introduction

Currently, the carbon cycles of terrestrial ecosystems have already been significantly influenced by global warming through altered water cycles [1,2]. Ecosystem-scale water-use efficiency (WUE), defined as the rate of carbon assimilation (e.g., gross primary productivity (GPP)) per unit of water loss (e.g., evapotranspiration (ET), which is the sum of evaporation and plant transportation from the Earth's land to the atmosphere), is an important indicator of ecological function and the coupled carbon-water cycle of terrestrial ecosystems [3,4]. A deeper understanding of how WUE has varied

and the related underlying regulatory mechanisms will provide valuable insight into how carbon and water cycles will change with future climate change [5].

To achieve this aim, temporal-spatial variations in WUE and their relationships with environmental factors, such as climatic factors, CO_2 concentration and nitrogen deposition, have been investigated by manipulation experiments, site and satellite observations, and data-driven and process-based ecosystem models [3,5–10]. However, the variations in WUE in response to biotic factors remain inadequately understood, and this will eventually result in uncertainties in modeling of global carbon and water budgets.

Phenology is the periodic plant life cycle, which includes not only the dates of life cycle events or phenomena (e.g., the sprouting and coloring of deciduous plants), but the state-transition times of annual cycles of ecosystem processes (e.g., the seasonality of photosynthesis in winter-dormant/summer-active evergreen ecosystems) [11]. From individual plants to the entire ecosystem, phenology directly or indirectly regulates carbon (e.g., photosynthesis and respiration) and water (e.g., transpiration and evaporation) fluxes between the land surface and the atmosphere [12] by altering physiological and structural characteristics, such as photosynthetic rate, canopy conductance, albedo and surface roughness, etc. [13].

Based on both ground observations and remotely sensed data, it has been widely reported that land surface phenology has significantly changed as a result of current climate change in terrestrial ecosystems of the Northern Hemisphere [13–19], and this modification is likely to affect processes of carbon and water cycles and consequent WUE [13,20–22]. However, phenology has not been fully considered in the regulation of WUE at the ecosystem scale. First, although previous studies have shown variations in WUE with phenology (e.g., leaf age and canopy leaf area index) at leaf scale [23–25], it is difficult to upscale these findings from leaf to ecosystem level [9]. Second, WUE responses to yearly anomalies in phenology for a range of plant functional types (PFTs) remain little understood [26]. It is well known that responses of carbon assimilation and uptake to variability of phenology vary with climate condition and plant type [12,27–29]. Due to the diverse sensitivities of carbon and water fluxes to interannual fluctuations of phenology, the variations in WUE with phenology can potentially be quite dynamic across PFTs [13]. Third, phenology may play different roles in regulating ecosystem processes. For example, the conceptual scenarios proposed by Richardson et al. [22] exhibited direct and/or indirect, positive and/or negative, and synchronized and/or lagged effects of earlier spring phenology on plant activities. Considering that a variability of WUE is determined by changes of both GPP and ET, the pattern by which WUE responds to phenology and the underlying mechanisms should be more complicated.

Taking into account the important role and future changes of phenology, awareness of temporal-spatial WUE responses to critical phenological factors in terrestrial ecosystems is critical and valuable. Remote sensing data are very useful for investigating long-term, large-scale variability of ecosystem-scale WUE from a real-world perspective [8,10]. This paper investigated sensitivities of ecosystem-scale WUE to phenological factors in the terrestrial ecosystems of the Northern Hemisphere during the past 14 years using satellite-based products, and tried to identify response patterns of WUE to phenology across different PFTs. Achieving these objectives is a helpful step toward improving our understanding and predictions of variabilities of carbon and water cycles.

2. Materials and Methods

2.1. Satellite-Based WUE Datasets

Datasets of MODIS monthly GPP and ET (MOD17A2 and MOD16A2, Version 055) at 1 km spatial resolution from 2001 to 2014 [30,31] were used to calculate the ecosystem-scale WUE, which is defined as the ratio of GPP ($g \cdot C \cdot m^{-2}$) to ET (mm) [4,9,10]. MODIS GPP and ET are derived from satellite-based vegetation information data along with meteorological data, using a light-use efficiency model [32,33] and the Penman–Monteith approach [34], respectively. It is reported that MODIS WUE

estimates compared favorably with tower-based measurements of WUE [8]. The monthly GPP and ET datasets were averaged to give seasonal mean for each year to a 0.5° grid [10]. In our analysis, the seasons concerned included spring, summer and autumn, defined as March-May, June-August and September-November, respectively.

2.2. Valid Pixels and Plant Functional Types

The yearly MODIS land cover type dataset (MCD12Q1, Collection 5.1 IGBP Land Cover) at 0.5° spatial resolution from 2001 to 2012 [35], as well as the aggregated GPP dataset, were used to identify the valid satellite-image pixels in the Northern Hemisphere. This involved using the following criteria: at least 10 years of data records of the constant land cover type; less than 20% gap of data records of GPP in each year; summer active ecosystem of which summer (June–August) GPP was the highest and winter (December–February) GPP was the lowest in an annual cycle. Additionally, non-vegetation types (e.g., built-up, barren) and permanent wetlands were also excluded. Then, each valid pixel was assigned to a plant functional type (PFT), which was defined by both the Köppen climate classification [36] and MODIS IGBP land cover type. For example, boreal evergreen needleleaf forests is referred to as D2-ENF, of which D2 indicates continental subarctic or boreal climates, and ENF indicates evergreen needleleaf forests (Table 1). After filtering, a total of 27,484 valid pixels within 33 PFTs in the Northern Hemisphere were included in our present work, and the details and spatial distribution of PFTs are shown in Table 1 and Figure 1.

Table 1. Descriptions of the climate and plant types in this study based on the Köppen climate classifications and the MODIS IGBP land cover types, respectively. The details regarding the codes of Köppen climate classifications are provided by Rubel and Kottek [36].

Climate Types	Köppen Climate Classifications	Plant Types	MODIS Land Cover Types
B	Dry (arid and semiarid) climates: *BWh/BWk/BSh/NSk*	ENF	Evergreen Needleleaf Forests
C1	Dry-summer or Mediterranean climates: *Csa/Csb*	EBF	Evergreen Broadleaf Forests
C2	Humid subtropical climates: *Cwa/Cfa*	DNF	Deciduous Needleleaf Forests
C3	Maritime temperate climates or Oceanic climates: *Cwb/Cwc/Cfb/Cfc*	DBF	Deciduous Broadleaf Forests
D1	Hot or warm summer continental climates or hemiboreal climates: *Dsa/Dsb/Dwa/Dwb/Dfa/Dfb*	MF	Mixed Forests
		SHR	Closed Shrublands, open Shrublands
D2	Continental subarctic or boreal climates (with extremely severe winters): *Dsc/Dsd/Dwc/Dwd/Dfc/Dfd*	WSA	Woody Savannas, savannas
		GRA	Grasslands
E	Polar and alpine climates: *ET*	CRO	Croplands, cropland/Natural vegetation mosaic

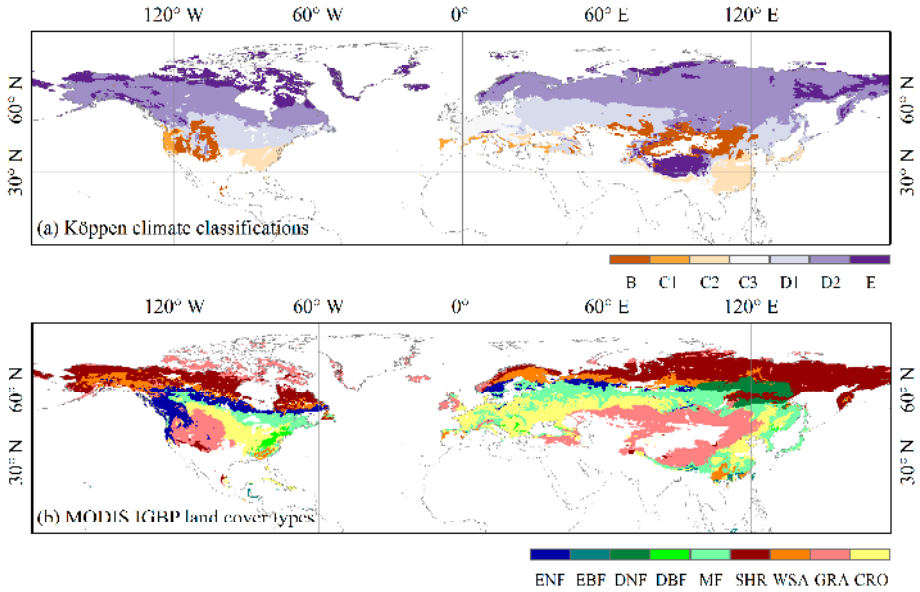

Figure 1. Spatial patterns of (**a**) Köppen climate classifications and (**b**) MODIS IGBP land cover types within the valid pixels of this study. The details regarding the codes of the climate and plant types are provided in Table 1. The white areas denote invalid satellite-image pixels in this study.

2.3. Meteorological Datasets

Environmental factors, including the mean air temperature (°C), total precipitation (mm), daily shortwave solar radiation ($MJ \cdot m^{-2} \cdot day^{-1}$) and atmospheric carbon dioxide concentration (CO_2, ppm), were considered as the abiotic controls of WUE in our analysis. For valid pixels, the seasonal temperature and precipitation from 2001 to 2014 were derived from the Centre for Environmental Data Analysis (CEDA) monthly temperature and precipitation dataset at 0.5° spatial resolution [37]. The seasonal solar radiation dataset at 0.5° spatial resolution was derived from the National Centers for Environmental Prediction (NECP) 4-times daily downward radiation data at 1.875° spatial resolution [38] by interpolation and aggregation. Due to limitations of data availability, the CO_2 concentration for each valid pixel was replaced by that measured daily at Mauna Loa (Hawaii) [39] during 2001–2014, and then was aggregated to seasonal mean data for each year.

2.4. GPP-Based Phenology

In this study, the spring and autumn state-transition dates of GPP-based photosynthesis cycle, referred as the start (SOS) and end (EOS) of growing season, were adopted rather than the traditional phenological events of the plants. These phenological factor dates were derived at different spatial scales. First, they were derived at the site scale using both the FLUXNET daily GPP flux measurements and the MODIS 8-day GPP dataset at 1 km spatial resolution [30] for comparison between the ground and satellite observed phenology. Then, the phenological factors were calculated in each valid satellite-image pixel using the 8-day GPP dataset at 0.5° spatial resolution which was derived from the MODIS 8-day GPP dataset at 1 km spatial resolution.

The Harmonic Analysis of Time Series (HANTS) model was used to smooth both the satellite-based and tower-based GPP measurements of each year. HANTS is an improved algorithm of the fast Fourier transform (FFT), which is described in detail in the work of Roerink et al. [40]. In this study, the HANTS algorithm was implemented in MATLAB R2013a (The Mathworks, Inc., Natick, MA, USA), and the code was provided by Mohammad Abouali [41]. For the algorithm, the number of frequencies is set to 1, the fit error tolerance is set to 5.0, and the degree of overdeterminedness is set to 1. Then, the smoothed GPP time series were used to define the SOS and EOS in each pixel-year (site-year) data, with the dates on which the smoothed daily GPP reached 10% of the seasonal maximum in spring

and autumn used to indicate the onset and end of significant photosynthesis, respectively (Figure 2a). This 10% GPP threshold was determined because dynamic thresholds are more beneficial for capturing and comparing interannual variations in phenological events [42].

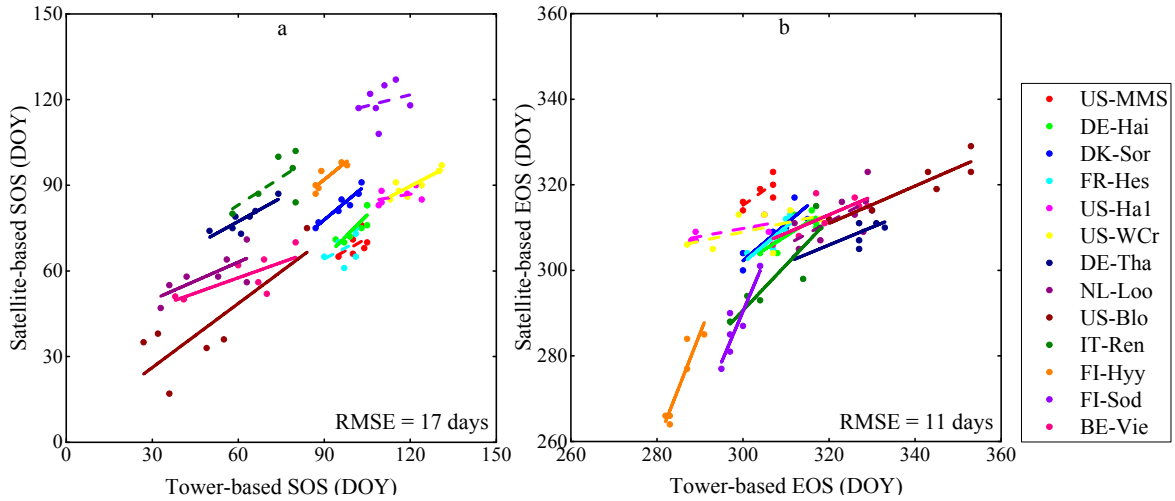

Figure 2. Comparison between the tower-based and satellite-based (**a**) start (SOS) and (**b**) end (EOS) of growing season at the FLUXNET sites and the corresponding MODIS 3 × 3 pixels. Solid and dash lines denote significant and no significant linear regression, respectively, between tower-based and satellite-based phenological factors. DOY denotes day of year. The details regarding the FLUXNET sites are provided in Table S1.

To validate satellite-derived photosynthetic phenology, 13 sites (a total of 85 site-years) in the FLUXNET (the "Fair Use" LaThuile FLUXNET data set (V4)) [43] were identified, and the daily GPP fluxes were derived from 30-min eddy covariance measurements (net ecosystem exchange of CO_2, NEE) that were standardized and gap-filled using a set of common algorithms [44,45]. Here, only summer active ecosystem sites which were identified by the same rule as the valid pixel were included in our analysis. In addition, the sites were filtered by data quality (less than 20% gap-filled records in each year; a lack of recent disturbances) and length of data record (a minimum of six years of continuous data since 2000). The details regarding these valid sites are provided in Table S1. According to the center geographic coordinates (latitude and longitude) of the selected field sites, the satellite-derived GPP time-series were extracted from 3 × 3 MODIS pixels (~3 km × ~3 km) centered on the flux tower [42].

2.5. Statistical Analysis Strategy

First, sensitivities of ecosystem-scale seasonal WUE to phenological factors were examined by Spearman partial correlation analysis for each valid pixel, after controlling for environmental factors (including temperature, precipitation, solar radiation and CO_2 concentration). Meanwhile, the variation in WUE in response to phenological and environmental factors at the PFT level was quantitatively identified by a panel (data) analysis [46] using a linear random-effects generalized least squares (GSL) regression model [47] across all pixels in each PFT. The partial correlation analysis and panel analysis were implemented in MATLAB R2013a (The Mathworks, Inc., Natick, MA, USA) and STATA 14 (StataCorp LP, College Station, TX, USA), respectively.

Then, response patterns of WUE to phenology were identified according to relationships of WUE and its components (GPP and ET) with the phenological factor (SOS or EOS). Here, six response patterns of WUE to phenology were defined by the partial correlation coefficients of R_{WUE} (WUE vs. phenology), R_{GPP} (GPP vs. phenology) and R_{ET} (ET vs. phenology), including $R_{WUE} < 0$, $R_{GPP} < 0$ and $R_{ET} < 0$ (Pattern I), $R_{WUE} < 0$, $R_{GPP} < 0$ and $R_{ET} > 0$ (Pattern II), $R_{WUE} < 0$, $R_{GPP} > 0$ and $R_{ET} > 0$

(Pattern III), $R_{WUE} > 0$, $R_{GPP} < 0$ and $R_{ET} < 0$ (Pattern IV), $R_{WUE} > 0$, $R_{GPP} > 0$ and $R_{ET} < 0$ (Pattern V) and $R_{WUE} > 0$, $R_{GPP} > 0$ and $R_{ET} > 0$ (Pattern VI).

3. Results

3.1. Validation of Satellite-Based Phenology

The method described in Section 2.4 was used to determine the SOS and EOS from both the tower-based and satellite-based GPP time-series at the site scale (Figure 2). The linear regression analysis showed that satellite-based SOS and EOS were positively correlated with tower-based SOS (Pearson's $r = 0.69 \pm 0.20$) and EOS (Pearson's $r = 0.80 \pm 0.12$) at all 13 study sites over the measurement period, and positive relationships for SOS and EOS were significant ($P < 0.05$) at 8 and 9 of the 13 sites, respectively. The corresponding RMSEs for SOS and EOS were nearly 17 and 11 days, respectively. Although the bias is expected to introduce inconsistence in the absolute dates of phenological transitions, this should not affect interannual fluctuation changes and long-term trends or the interannual relationships of fluxes with phenology for each site or satellite pixel [28].

3.2. Partial Correlations between WUE and Phenological Factors

Figure 3 provides the spatial distributions of coefficients of partial correlation (r) between yearly fluctuations of seasonal WUE and phenological factors during 2001–2014, where r is significant when the absolute value of r is higher than 0.60. Negative partial correlations between WUE and SOS (i.e., WUE enhanced with earlier SOS or WUE decreased with later SOS) dominate the spring (96.08% pixels), and 67.33% of these are statistically significant ($P < 0.05$) mainly in the mid- and high latitudes (over 50°N), southwestern China and mid-western North America (Figure 3a). At the PFT level, our statistics show in general, the negative partial correlations between spring WUE and SOS enhance from warm climates to cold climates (Figure 4a). The PFT-level average partial correlation coefficient between them ranges from -0.28 in dry climates (B) to -0.80 in continental subarctic climates (D2), with the strongest correlation of -0.87 (± 0.10) in D2-WSA. The panel analysis shows similar results (Table S2). When SOS advances a 10-day, the spring WUE will increase on average by 0.05, 0.04, 0.21 and 0.06 $g{\cdot}C{\cdot}m^{-2}{\cdot}mm^{-1}$ in dry climates (B), temperate/mesothermal climates (C1, C2 and C3), continental/microthermal climates (D1 and D2) and Polar and alpine climates (E), respectively.

During summer, both negative and positive correlations between WUE and SOS are found (Figure 3b), with 16.64% of valid pixels having significant negative correlations ($P < 0.05$) mainly at high latitudes (e.g., northern Siberia, northeastern Canada and mid-western United States) and 4.14% significant positive correlations ($P < 0.05$) mainly in mid-eastern United States, most Europe, north-eastern China and central Siberia. D1-DBF shows the strongest positive partial correlations between summer WUE and SOS with a coefficient of 0.45 (± 0.28) (Figure 4b), and decreases by an average value of 0.11 (± 0.01) $g{\cdot}C{\cdot}m^{-2}{\cdot}mm^{-1}$ with a 10-day advancement of SOS (Table S2). E-SHR and D2-SHR show the strongest negative partial correlation ($r = -0.51 \pm 0.28$) (Figure 4b) and the lowest regression coefficient of panel analysis (coef = -0.15 $g{\cdot}C{\cdot}m^{-2}{\cdot}mm^{-1}$ 10-day^{-1}) between summer WUE and SOS, respectively (Table S2), indicating significant promotions of earlier SOS to summer WUE in extreme cold regions.

Positive correlations between autumn WUE and EOS are mainly observed in 86.67% of valid pixels (Figure 3c), and 32.40% of these are statistically significant ($P < 0.05$) mainly at high latitudes (e.g., northern North America and northern Eurasia). Similar to spring, the partial correlations between autumn WUE and EOS of PFTs in cold regions are generally stronger than those in warm areas (Figure 4c). However, the correlations are weaker overall, ranging from 0.12 in humid subtropical climates (C2) to 0.43 in continental subarctic climates (E) on average. Moreover, some areas with a significant correlation in spring (e.g., eastern North America, north Europe and West Siberia) exhibit no significant correlation in the autumn, indicating differences in ecological effects of different phenological changes observed in a changing climate.

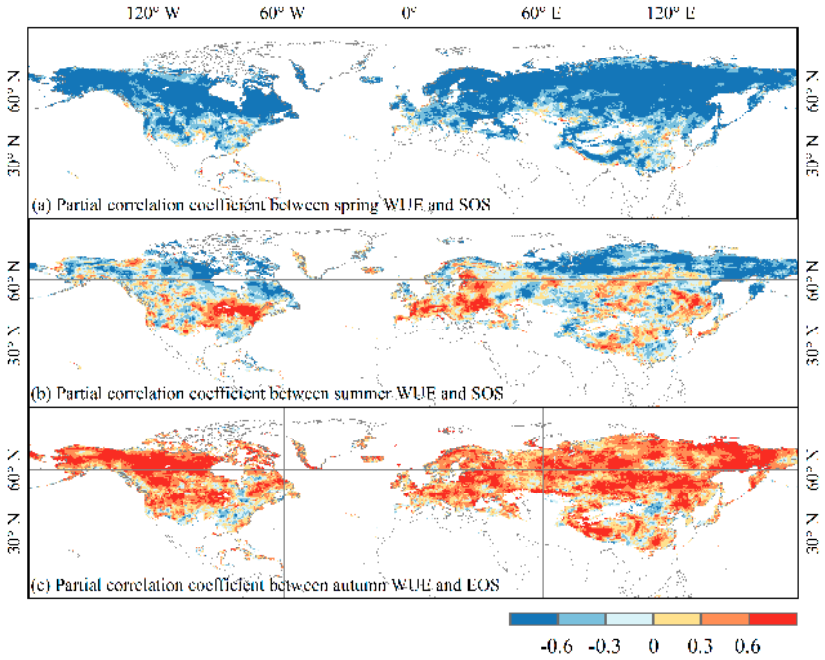

Figure 3. Spatial distribution of partial correlation coefficients between the phenological factor (SOS/EOS) and water-use efficiency (WUE) during (**a**) spring (March–May); (**b**) summer (June–August) and (**c**) autumn (September–November) during 2001–2014. Partial correlation coefficient is calculated after controlling the environmental factors (including temperature, precipitation, insolation and CO_2 concentration), which is significant ($P < 0.05$) when the absolute value of coefficient is higher than 0.60. The white areas denote invalid satellite-image pixels in this study.

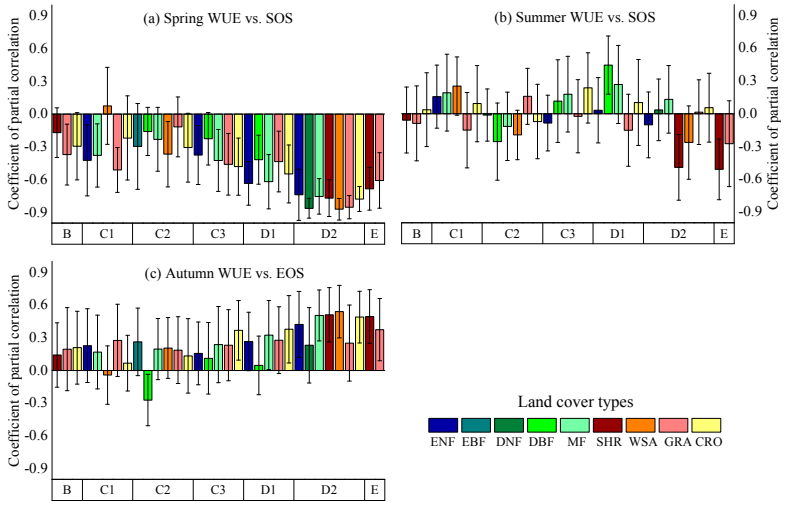

Figure 4. Relationships between the phenological factor (SOS/EOS) and WUE during (**a**) spring (March–May); (**b**) summer (June–August) and (**c**) autumn (September–November) at the plant functional type (PFT) level. Partial correlation coefficient is calculated after controlling the environmental factors (including temperature, precipitation, insolation and CO_2 concentration), which is significant ($P < 0.05$) when the absolute value of coefficient is higher than 0.60. The x-axis and color indicate the climate types and plant types of PFTs, respectively, and the details regarding the codes of PFTs are provided in Table 1.The bar indicates the mean partial correlation coefficient (±standard error) for each PFT.

3.3. Response Patterns of WUE to Phenology

Here, spatial distributions of the six response patterns of WUE to photosynthetic phenology are shown in Figure 5. The results show that Pattern I ($R_{WUE} < 0$, $R_{GPP} < 0$, $R_{ET} < 0$) and Pattern II ($R_{WUE} < 0$, $R_{GPP} < 0$, $R_{ET} > 0$) are widespread (about 54.87% and 36.83% of the valid pixels, respectively) in the high and mid latitudes during spring (Figure 5a). This indicates that the negative response of spring WUE to the advance in SOS is mainly because the negative sensitivity of GPP to SOS is relatively strong in magnitude compared to that of ET, or GPP negatively responds to SOS while ET positively responds to SOS during spring. In other words, an increasing spring WUE with earlier SOS, for example, is mainly shown by a steeper increase in GPP than ET, or by an increase in GPP accompanied by a decrease in ET resulting from an advance in SOS. However, for some PFTs in dry or Mediterranean climates (e.g., B-SHR and C1-WSA) (Figure 6a), both spring GPP and ET exhibit a positive correlation with variations in SOS, leading to an increase or decrease in WUE according to their changing magnitudes.

The response patterns of summer WUE to SOS give a different picture (Figure 5b), with only 15.05% and 27.13% of pixels showing Pattern I ($R_{WUE} < 0$, $R_{GPP} < 0$, $R_{ET} < 0$) and Pattern II ($R_{WUE} < 0$, $R_{GPP} < 0$, $R_{ET} > 0$), respectively, mainly in regions of north of 60°N, northeastern Canada and East and South China. Areas with Pattern III ($R_{WUE} < 0$, $R_{GPP} > 0$, $R_{ET} > 0$) and Pattern VI ($R_{WUE} > 0$, $R_{GPP} > 0$, $R_{ET} > 0$) (about 20.00% and 18.98% of the valid pixels, respectively) are widespread in the mid latitudes (including most PFTs in dry climates, Mediterranean climates and continental climates with warm summers) (Figure 6b), indicating that summer GPP and ET positively respond to advance in SOS, whereas summer WUE increases or decreases are determined by the changing magnitudes of GPP and ET.

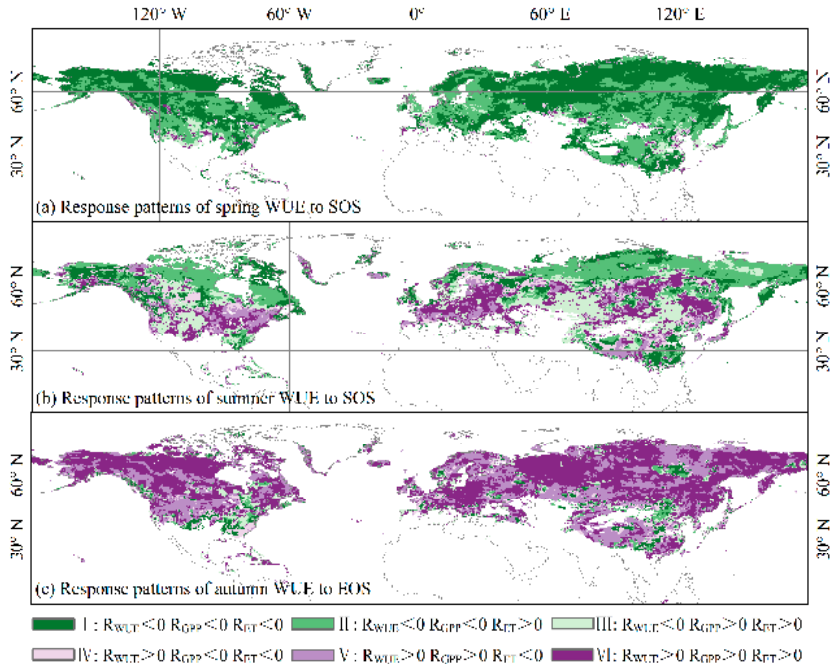

Figure 5. Spatial distribution of response patterns of seasonal WUE to phenological factors (SOS/EOS). R_{WUE}, R_{GPP}, R_{ET} indicate the partial correlation coefficients of WUE, gross primary productivity (GPP), evapotranspiration (ET) with the phenological factor after controlling the environmental factors (including temperature, precipitation, insolation and CO_2 concentration), respectively. The partial correlation coefficients are calculated in (**a**) spring (March–May); (**b**) summer (June–August) and (**c**) autumn (September–November), respectively. The white areas denote invalid satellite-image pixels in this study.

During autumn, Pattern VI ($R_{WUE} > 0$, $R_{GPP} > 0$, $R_{ET} > 0$) and Pattern V ($R_{WUE} > 0$, $R_{GPP} > 0$, $R_{ET} < 0$) are observed in 50.61% and 31.16% of valid pixels, respectively (Figure 5c). These response patterns of autumn WUE to EOS indicate that an increased autumn WUE resulting from a delayed EOS is mainly associated with an enhanced GPP, with either a relatively slight increase in ET or a decrease in ET. Nevertheless, in parts of central United States, Inner Mongolia and southwest China and east Siberia, the contrast patterns are observed; there is a negative relationship between autumn WUE, and EOS is associated to with a negative correlation of autumn GPP with EOS.

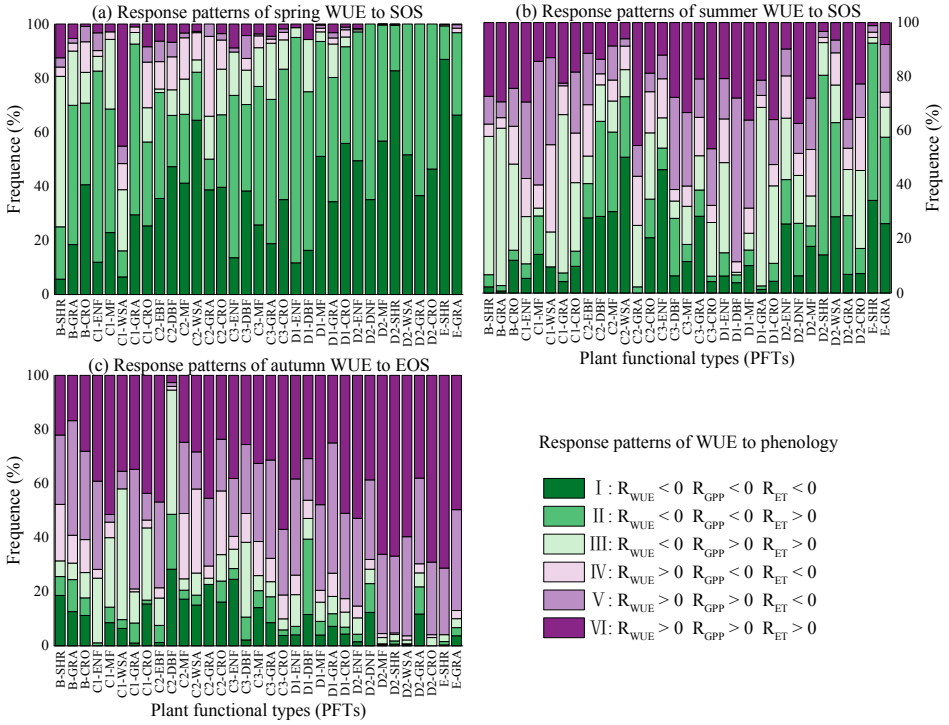

Figure 6. Frequency distribution of response patterns of seasonal WUE to phenological factors (SOS/EOS) at plant functional type (PFT) level. R_{WUE}, R_{GPP}, R_{ET} indicate the partial correlation coefficient of WUE, GPP, ET with phenological factor after controlling the environmental factors (including temperature, precipitation, insolation and CO_2 concentration). The partial correlation coefficients are calculated in (**a**) spring (March–May); (**b**) summer (June–August) and (**c**) autumn (September–November), respectively. The details regarding the codes of PFTs are provided in Table 1.

4. Discussion

4.1. WUE Responses to Phenology

Our analysis shows that WUE sensitivity to phenology exhibits an obvious difference among different PFTs, and further highlights that the difference varies with the season. During spring, WUE sensitivity to phenology gradually enhances from PFTs in warm climates to those in cold climates. This result is in agreement with the fact that ecological functions seem to be more sensitive in cold-habitat and alpine ecosystems compared to warm-habitat ones [48,49]; this may be because there are fewer but longer days of growing season at higher latitudes [50]. Although the sensitivities of PFTs in similar climates also show a variance, the amplitude of variance is much less than that in different climates, indicating fundamental similarities in ecosystem functioning across a broad geographic range of climate conditions, with the different sensitivities of different plant types [51].

WUE response to phenology, indeed, is the coupling of GPP and ET responses to phenology. Our analysis shows different response patterns of WUE to phenology, and here are some potential cues to explain how GPP and ET responds to phenology:

(1) During spring, increases in WUE with earlier SOS are generally associated with increases in GPP with advanced SOS. Warmer spring air temperature can trigger leaf sprouting and unfolding [28]. Thus, increases in productivity are driven by the longer growing season (earlier SOS). Moreover, an earlier spring phenology may result in greater leaf area, enhancing light interception and canopy-level photosynthetic potential and thereby spring GPP [52]. Both negative and positive correlations between ET and SOS are widespread during spring. The spring onsets represents a release from temperature limitation, but it is generally still not warm enough to have large evaporative losses from soil. Transpiration will be the larger contributor to ET at this time of year. On the one hand, the transpiration of the leaves and canopy interception evaporation would increase with the greater leaf area at the beginning of the growing season [53], which could increase ecosystem ET. Meanwhile, warmer spring temperatures could increase soil evaporation during the early growing season, accompanying an earlier spring phenology [54]. On the other hand, an earlier and/or greater display of leaf area can decrease soil evaporation resulting from lower local temperatures [29,55] and land surface insolation [56]. The offset of these effects determines the relationship between spring ET and SOS, which would imply Pattern I or Pattern II in spring.

(2) In summer, an advance in SOS also promotes GPP in humid subtropical climates and subarctic climates, which is probably attributed to higher foliar N or leaf area index resulting from warmer spring temperature [57,58], which would also imply Pattern I or Pattern II. However, positive correlations between summer GPP and SOS are mainly observed during summer, especially in dry climates and continental climates. These positive relationships (that is, earlier SOS reducing summer GPP) may be attributed to water stress resulting from the preseason environmental condition [54,59] and/or from the enhanced plant activity during the warm spring [1,54]. In this case, summer ET may not increase if leaf transpiration and soil evaporation are limited by soil water availability [13], and so it exhibits a positive correlation with SOS. The decrease in GPP and ET due to earlier SOS linked with summer water deficit would imply Pattern III or Pattern VI.

(3) Similar to spring, a longer growing season (later EOS) promotes autumn GPP, and might cause plants to close stomates and increase WUE because soil moisture deficit at this time of year is common. On the contrary, in some areas of United States, China and high latitudes (around 60° N), temperature and solar radiation during autumn tend to be negatively correlated, and warming would likely bring more cloudy weather and less insolation [60]. Hence, carbon assimilation may be limited by photosynthetically active radiation despite of an extended growing season [61], showing a negative relationship between autumn GPP and EOS. Besides, the offset between soil evaporation and leaf transpiration influenced by temperature and insolation determines the increase or decrease in autumn ET. This simultaneous decrease in GPP and ambiguous ET would imply Pattern I or Pattern II in autumn.

Huang et al. [4] have investigated variability of ecosystem-scale WUE at global scale using data-driven and process-oriented models and flux data, and showed that the seasonal variation of WUE trends is primarily attributable to effects of seasonal climatic variables. Here, our study further highlights that WUE during spring and autumn are extensively and significantly sensitive to phenology after statistically controlling for the climatic variables and CO_2 concentration. Even though during the summer WUE is also significantly affected by SOS in parts of regions with continental and subarctic climates. This demonstrates that phenology plays a crucial role in the regulation of ecosystem WUE, which should not be ignored in earth system models [13].

4.2. Uncertainties and Further Studies

Previous studies have reported that MODIS produces a systematic error for GPP and ET and WUE is compared to other satellite-based products (e.g., JUNG flux products, see [62]) due to the algorithms in tropical regions [10]. With this point, only summer active ecosystems in extratropical areas were taken into account in this study, which is helpful in reducing the uncertainty around the

findings. In further studies, multi-source data, as well as model simulation, are helpful to improve on our present analysis to characterize robust relationships between WUE and phenology. Additionally, more ecosystems should be comprehensively considered across climatic gradients, especially those where greening is closely associated with water supplement availability [63].

Mismatch between ground- and satellite-observed phenology is always a difficult question in phenology research due to temporal and spatial scales, mixed pixel, etc. For the validation of satellite-based phenology, it is more appropriate that the comparison is made using interannual fluctuation changes or long-term trends rather than actual dates [28]. Moreover, an ensemble of diverse algorithms is helpful to reduce uncertainties in phenology modeling [42].

Ecosystem-scale WUE response to nitrogen availability is not considered in our present work. It is reported that photosynthetic rates and stomatal conductance to water vapor may be stimulated by increased deposition of reactive nitrogen (e.g., resulting from human activities) in nitrogen-limited ecosystems [64–66]. Although little contribution of nitrogen deposition to the variability of seasonal WUE was reported [4], it is helpful to take effects of nitrogen deposition into account in further studies to improve on the present analysis.

Agricultural ecosystem is included in our analysis. However, it is worth noting that although there are not clear differences in WUE response to phenology between agricultural and other ecosystems, some uncertainties in the results may be caused by data quality [67] and human management (e.g., anomaly in phenology due to planting and harvesting, as well as that in carbon and water flux due to fertilization and irrigation). Hence, more detailed investigations into agricultural WUE response to phenology will be needed.

5. Conclusions

Our study investigated interannual relationships between ecosystem-scale WUE during the different seasons and the photosynthetic phenological factors in summer-active ecosystems of the Northern Hemisphere, and identified patterns of WUE response to phenology as well as dominant control on WUE. We find that the WUE during spring and autumn closely relates to the start and end dates of growing season, respectively, over most of the study area. Meanwhile, the main pattern of WUE response to phenology suggests that during spring (or autumn), an increasing WUE with an advancing SOS (or a delaying EOS) is mainly attributed to a steeper increase in GPP relative to increase in ET, because of the higher phenological sensitivity of GPP relative to ET. However, summer WUE was weakly related to SOS during the study period. In summary, we argue that phenology plays an important role in the regulation of terrestrial ecosystem water-use efficiency, and it is necessary to take into account phenological factors when explaining and predicting patterns of the coupled carbon-water cycle of territorial ecosystems.

Supplementary Materials: The following are available online at www.mdpi.com/2072-4292/9/7/664/s1, Table S1: Info of the valid FLUXNET sites in this study, Table S2: Variations in seasonal WUE with the phenological factors for each PFT through the panel analysis.

Acknowledgments: This work was supported by the National Natural Science Foundation of China (No. 41601442); the Jiangsu Provincial Natural Science Foundation of China (No. BK20150579); and the China Postdoctoral Science Foundation (No. 2016T90442 & 2015M57043). We thank the Numerical Terradynamic Simulation Group at the University of Montana, the Centre for Environmental Data Analysis, The National Centers for Environmental Prediction and the Earth System Research Laboratory to provide satellite-derived product and climate data. This work used eddy covariance data acquired by the FLUXNET community and in particular by the following networks: AmeriFlux, CarboEurope-IP and Fluxnet-Canada.

Author Contributions: Jiaxin Jin and Hong Jiang had the original idea for the study and designed the research. Jiaxin Jin, Ying Wang and Ming Cheng analyzed the data. Jiaxin Jin drafted the manuscript, which was revised by all authors. All authors read and approved the final manuscript.

Conflicts of Interest: The authors declare no conflict of interest.

References

1. Hufkens, K.; Keenan, T.F.; Flanagan, L.B.; Scoot, R.L.; Bernacchi, C.J.; Joo, E.; Brunsell, N.A.; Verfaillie, J.; Richardson, A.D. Productivity of North American grasslands is increased under future climate scenarios despite rising aridity. *Nat. Clim. Chang.* **2016**, *6*, 710–714. [CrossRef]
2. Wolf, S.; Keenan, T.F.; Fisher, J.B.; Baldocchi, D.D.; Desai, A.R.; Richardson, A.D.; Scott, R.L.; Law, B.E.; Litvak, M.E.; Brunsell, N.A.; et al. Warm spring reduced carbon cycle impact of the 2012 US summer drought. *Proc. Natl. Acad. Sci. USA* **2016**, *113*, 5880–5885. [CrossRef] [PubMed]
3. Keenan, T.F.; Hollinger, D.Y.; Bohrer, G.; Dragoni, D.; Munger, J.W.; Schmid, H.P.; Richardson, A.D. Increase in forest water-use efficiency as atmospheric carbon dioxide concentrations rise. *Nature* **2013**, *499*, 324–327. [CrossRef] [PubMed]
4. Huang, M.; Piao, S.; Zeng, Z.; Peng, S.; Chais, P.; Cheng, L.; Mao, J.; Poulter, B.; Shi, X.; Yao, Y.; et al. Seasonal responses of terrestrial ecosystem water-use efficiency to climate change. *Glob. Chang. Biol.* **2016**, *22*, 2165–2177. [CrossRef] [PubMed]
5. Niu, S.; Xing, X.; Zhang, Z.; Xia, J.; Zhou, X.; Song, B.; Li, L.; Wan, S. Water-use efficiency in response to climate change: From leaf to ecosystem in a temperate steppe. *Glob. Chang. Biol.* **2011**, *17*, 1073–1082. [CrossRef]
6. Yu, G.; Song, X.; Wang, Q.; Liu, Y.; Guan, D.; Yan, J.; Sun, X.; Zhang, L.; Wen, X. Water-use efficiency of forest ecosystems in eastern China and its relations to climatic variables. *New Phytol.* **2008**, *177*, 927–937. [CrossRef] [PubMed]
7. Dong, G.; Guo, J.; Chen, J.; Sun, G.; Gao, S.; Hu, L.; Wang, Y. Effects of spring drought on carbon sequestration, evapotranspiration and water use efficiency in the Songnen meadow steppe in northeast china. *Ecohydrology* **2011**, *4*, 211–224. [CrossRef]
8. Tang, X.; Li, H.; Desai, A.R.; Nagy, Z.; Luo, J.; Kolb, T.E.; Olioso, A.; Xu, X.; Yao, L.; Kutsch, W.; et al. How is water-use efficiency of terrestrial ecosystems distributed and changing on Earth? *Sci. Rep.* **2014**, *4*, 7483. [CrossRef] [PubMed]
9. Huang, M.; Piao, S.; Sun, Y.; Ciais, P.; Cheng, L.; Mao, J.; Poulter, B.; Shi, X.; Zeng, Z.; Wang, Y. Change in terrestrial ecosystem water-use efficiency over the last three decades. *Glob. Chang. Biol.* **2015**, *21*, 2366–2378. [CrossRef] [PubMed]
10. Sun, Y.; Piao, S.; Huang, M.; Ciais, P.; Zeng, Z.; Cheng, L.; Li, X.; Zhang, X.; Mao, J.; Peng, S.; et al. Global patterns and climate drivers of water-use efficiency in terrestrial ecosystems deduced from satellite-based datasets and carbon cycle models. *Glob. Ecol. Biogeogr.* **2016**, *25*, 311–323. [CrossRef]
11. Morisette, J.T.; Richardson, A.D.; Knapp, A.K.; Fisher, J.I.; Graham, E.A.; Abatzoglou, J.; Wilson, B.E.; Breshears, D.D.; Henebry, G.M.; Hanes, J.M.; et al. Tracking the rhythm of the seasons in the face of global change: Phenological research in the 21st century. *Front. Ecol. Environ.* **2009**, *7*, 253–260. [CrossRef]
12. Noormets, A. (Ed.) *Phenology of Ecosystem Processes*; Springer: New York, NY, USA, 2009.
13. Richardson, A.D.; Keenan, T.F.; Migliavacca, M.; Ryu, Y.; Sonnentag, O.; Toomey, M. Climate change, phenology, and phenological control of vegetation feedbacks to the climate system. *Agric. For. Meteorol.* **2013**, *169*, 156–173. [CrossRef]
14. Fu, Y.; Piao, S.; Vitasse, Y.; Zhao, H.; Boech, H.J.D.; Liu, Q.; Yang, H.; Weber, U.; Hänninen, H.; Janssens, I.A. Increased heat requirement for leaf flushing in temperate woody species over 1980–2012: Effects of chilling, precipitation and insolation. *Glob. Chang. Biol.* **2015**, *21*, 2687–2697. [CrossRef] [PubMed]
15. Fu, Y.; Zhao, H.; Piao, S.; Peaucelle, M.; Peng, S.; Zhou, G.; Ciais, P.; Huang, M.; Menzel, A.; Peñuelas, J.; et al. Declining global warming effects on the phenology of spring leaf unfolding. *Nature* **2015**, *526*, 104–107. [CrossRef] [PubMed]
16. Piao, S.; Tan, J.; Chen, A.; Fu, Y.H.; Ciais, P.; Liu, Q.; Janssens, I.A.; Vicca, S.; Zeng, Z.; Jeong, S.J.; et al. Leaf onset in the northern hemisphere triggered by daytime temperature. *Nat. Commun.* **2015**, *6*, 6911. [CrossRef] [PubMed]
17. Ge, Q.; Wang, H.; Rutishauser, T.; Dai, J. Phenological response to climate change in China: A meta-analysis. *Glob. Chang. Biol.* **2015**, *21*, 265–274. [CrossRef] [PubMed]
18. Dai, J.; Wang, H.; Ge, Q. The spatial pattern of leaf phenology and its response to climate change in China. *Int. J. Biomteorol.* **2014**, *58*, 521–528. [CrossRef] [PubMed]

19. Wang, H.; Ge, Q.; Rutishauser, T.; Dai, Y.; Dai, J. Parameterization of temperature sensitivity of spring phenology and its application in explaining diverse phenological responses to temperature change. *Sci. Rep.* **2015**, *5*, 8833. [CrossRef] [PubMed]
20. Bonan, G.B. Forests and Climate Change: Forcings, Feedbacks, and the Climate Benefits of Forests. *Science* **2008**, *320*, 1444–1449. [CrossRef] [PubMed]
21. Peñuelas, J.; Rutishauser, T.; Filella, I. Phenology feedbacks on climate change. *Science* **2009**, *324*, 887–888. [CrossRef] [PubMed]
22. Richardson, A.D.; Black, T.A.; Ciais, P.; Delbart, N.; Fried, M.A.; Gobron, N.; Hollinger, D.Y.; Kutsch, W.L.; Longdoz, B.; Luyssaert, S.; et al. Influence of spring and autumn phenological transitions on forest ecosystem productivity. *Philos. Trans. R. Soc. Lond. Ser. B* **2010**, *365*, 3227–3246. [CrossRef] [PubMed]
23. Sobrado, M.A. Leaf age effects on photosynthetic rate, transpiration rate and nitrogen content in a tropical dry forest. *Physiol. Plant.* **1994**, *90*, 210–215. [CrossRef]
24. Muthuri, C.W.; Ong, C.K.; Craigon, J.; Mati, B.M.; Ngumi, V.W.; Black, C.R. Gas exchange and water use efficiency of trees and maize in agroforestry systems in semi-arid kenya. *Agric. Ecosyst. Environ.* **2009**, *129*, 497–507. [CrossRef]
25. Singh, N.; Patel, N.R.; Bhattacharya, B.K.; Soni, P.; Parida, B.R.; Parihar, J.S. Analyzing the dynamics and inter-linkages of carbon and water fluxes in subtropical pine (pinus roxburghii) ecosystem. *Agric. For. Meteorol.* **2014**, *197*, 206–218. [CrossRef]
26. Jin, J.; Zhan, W.; Wang, Y.; Gu, B.; Wang, W.; Jiang, H.; Lu, X.; Zhang, X. Water use efficiency in response to interannual variations in flux-based photosynthetic onset in temperate deciduous broadleaf forests. *Ecol. Indic.* **2017**, *79*, 122–127. [CrossRef]
27. Schwartz, M.D. (Ed.) *Phenology: An Integrative Environmental Science*; Springer: New York, NY, USA, 2013.
28. Keenan, T.F.; Gray, J.; Friedl, M.A.; Toomey, M.; Bohrer, G.; Hollinger, D.Y.; Mungre, J.W.; O'Keefe, J.; Schmid, H.P.; Wing, I.S.; et al. Net carbon uptake has increased through warming-induced changes in temperate forest phenology. *Nat. Clim. Chang.* **2014**, *4*, 598–604. [CrossRef]
29. Shen, M.; Piao, S.; Jeong, S.J.; Zhou, L.; Zeng, Z.; Ciais, P.; Chen, D.; Huang, M.; Jin, C.; Li, L.Z.X.; et al. Evaporative cooling over the Tibetan Plateau induced by vegetation growth. *Proc. Natl. Acad. Sci. USA* **2015**, *112*, 9299–9304. [CrossRef] [PubMed]
30. MODIS GPP/NPP Project (MOD17). Available online: http://www.ntsg.umt.edu/project/mod17 (accessed on 10 April 2015).
31. MODIS Global Evapotranspiration Project (MOD16). Available online: http://www.ntsg.umt.edu/project/mod16 (accessed on 10 April 2015).
32. Running, S.W.; Nemani, R.R.; Heinsch, F.A.; Zhao, M.; Reeves, M.; Hashimoto, H. A continuous satellite-derived measure of global terrestrial primary production. *BioScience* **2004**, *54*, 547–560. [CrossRef]
33. Zhao, M.; Heinsch, F.A.; Nemani, R.R.; Running, S.W. Improvements of the MODIS terrestrial gross and net primary production global data set. *Remote Sens. Environ.* **2005**, *95*, 164–176. [CrossRef]
34. Mu, Q.; Zhao, M.; Running, S.W. Improvements to a MODIS global terrestrial evapotranspiration algorithm. *Remote Sens. Environ.* **2011**, *115*, 1781–1800. [CrossRef]
35. MODIS Land Cover (MCD12Q1 Collection 5.1 IGBP Land Cover). Available online: http://glcf.umd.edu/data/lc (accessed on 3 December 2015).
36. Rubel, F.; Kottek, M. Observed and projected climate shifts 1901–2100 depicted by world maps of the Köppen-Geiger climate classification. *Meteorol. Z.* **2010**, *19*, 135–141. [CrossRef]
37. Centre for Environmental Data Analysis (CEDA). Available online: http://badc.nerc.ac.uk (accessed on 24 June 2016).
38. Earth System Researcher Laboratory: NCEP/NCAR Reanalysis 1. Available online: https://www.esrl.noaa.gov/psd/data/gridded/data.ncep.reanalysis (accessed on 18 July 2016).
39. Global Greenhouse Gas Reference Network: Trends in Atmospheric Carbon Dioxide. Available online: https://www.esrl.noaa.gov/gmd/ccgg/trends/data (accessed on 4 July 2016).
40. Roerink, G.J.; Menenti, M.; Verhoef, W. Reconstructing cloudfree NDVI composites using Fourier analysis of time series. *Int. J. Remote Sens.* **2000**, *21*, 1911–1917. [CrossRef]
41. MATLAB Implementation of Harmonic ANalysis of Time Series (HANTS) (Version 1.0). Available online: https://mabouali.wordpress.com/projects/harmonic-analysis-of-time-series-hants/ (accessed on 12 February 2014).

42. Wu, C.; Peng, D.; Soudani, K.; Siebicke, L.; Gough, C.M.; Arain, M.A.; Bohrer, G.; Lafleur, P.M.; Peichl, M.; Gonsamo, A.; et al. Land surface phenology derived from normalized difference vegetation index (NDVI) at global FLUXNET sites. *Agric. For. Meteorol.* **2016**, *233*, 171–182. [CrossRef]
43. The LaThuile FLUXNET Synthesis Dataset. Available online: http://www.fluxdata.org (accessed on 25 August 2014).
44. Papale, D.; Reichstein, M.; Aubinet, M.; Canfora, E.; Bernhofer, C.; Kutsch, W.; Longdoz, B.; Rambal, S.; Valentini, R.; Vesala, T.; et al. Towards a standardized processing of net ecosystem exchange measured with eddy covariance technique: Algorithms and uncertainty estimation. *Biogeosciences* **2006**, *3*, 571–583. [CrossRef]
45. Moffat, A.M.; Papale, D.; Reichstein, M.; Hollinger, D.Y.; Richardson, A.D.; Barr, A.G.; Beckstein, C.; Braswell, B.H.; Churkina, G.; Desai, A.R.; et al. Comprehensive comparison of gap-filling techniques for eddy covariance net carbon fluxes. *Agric. For. Meteorol.* **2007**, *147*, 209–232. [CrossRef]
46. Debarsy, N.; Ertur, C.; LeSage, J.P. Interpreting dynamic space-time panel data models. *Stat. Methodol.* **2012**, *9*, 158–171. [CrossRef]
47. Wu, Y.; Gu, B.; Erisman, J.W.; Reis, S.; Fang, Y.; Lu, X.; Zhang, X. PM2.5 pollution is substantially affected by ammonia emissions in China. *Environ. Pollut.* **2016**, *218*, 86–94. [CrossRef] [PubMed]
48. Piao, S.; Friedlingstein, P.; Ciais, P.; Viovy, N.; Demarty, J. Growing season extension and its impact on terrestrial carbon cycle in the northern hemisphere over the past 2 decades. *Glob. Biogeochem. Cycles* **2007**, *21*, 1148–1154. [CrossRef]
49. Seddon, A.W.R.; Macias-Fauria, M.; Long, P.R.; Benz, D.; Willis, K.J. Sensitivity of global terrestrial ecosystems to climate variability. *Nature* **2016**, *531*, 229–232. [CrossRef] [PubMed]
50. Ensminger, I.; Schmidt, L.; Lloyd, J. Soil temperature and intermittent frost modulate the rate of recovery of photosynthesis in Scots pine under simulated spring conditions. *New Phytol.* **2008**, *177*, 428–442. [CrossRef] [PubMed]
51. Churkina, G.; Schimel, D.; Braswell, B.H.; Xiao, X. Spatial analysis of growing season length control over net ecosystem exchange. *Glob. Chang. Biol.* **2005**, *11*, 1777–1787. [CrossRef]
52. Luyssaert, S.; Janssens, I.A.; Sulkava, M.; Papale, D.; Dolman, A.J.; Reichstein, M.; Hollmen, J.; Martin, J.G.; Suni, T.; Vesala, T.; et al. Photosynthesis drives anomalies in net carbon-exchange of pine forests at different latitudes. *Glob. Chang. Biol.* **2007**, *13*, 2110–2127. [CrossRef]
53. Zha, T.; Barr, A.G.; van der Kamp, G.; Black, T.A.; McCaughey, J.H.; Flanagan, L.B. Interannual variation of evapotranspiration from forest and grassland ecosystems in western Canada in relation to drought. *Agric. For. Meteorol.* **2010**, *150*, 1476–1484. [CrossRef]
54. Kljun, N.; Black, T.A.; Griffis, T.J.; Barr, A.G.; Gaumont-Guay, D.; Morgenstern, K.; McCaughey, J.H.; Nesic, Z. Response of net ecosystem productivity of three boreal forest stands to drought. *Ecosystems* **2006**, *9*, 1128–1144. [CrossRef]
55. Von Arx, G.; Dobbertin, M.; Rebetez, M. Spatio-temporal effects of forest canopy on understory microclimate in a long-term experiment in Switzerland. *Agric. For. Meteorol* **2012**, *166–167*, 144–155. [CrossRef]
56. Beer, C.; Ciais, P.; Reichstein, M.; Baldocchi, D.; Law, B.E.; Papale, D.; Soussana, J.F.; Ammann, C.; Buchmann, N.; Frank, D.; et al. Temporal and among-site variability of inherent water use efficiency at the ecosystem level. *Glob. Biogeochem. Cycles* **2009**, *23*, GB2018. [CrossRef]
57. Melillo, J.M.; Steudler, P.A.; Aber, J.D.; Newkirk, K.; Lux, H.; Bowles, F.P.; Catricala, C.; Magill, A.; Ahrens, T.; Morrisseau, S. Soil warming and carbon-cycle feedbacks to the climate system. *Science* **2002**, *298*, 2173–2176. [CrossRef] [PubMed]
58. Richardson, A.D.; Hollinger, D.Y.; Dail, D.B.; Lee, J.T.; Munger, J.W.; O'Keefe, J. Influence of spring phenology on seasonal and annual carbon balance in two contrasting New England forests. *Tree Physiol.* **2009**, *29*, 321–331. [CrossRef] [PubMed]
59. Hu, J.; Moore, D.J.P.; Burns, S.P.; Monson, R.K. Longer growing seasons lead to less carbon sequestration by a subalpine forest. *Glob. Chang. Biol.* **2010**, *16*, 771–783. [CrossRef]
60. Vesala, T.; Launiainen, S.; Kolari, P.; Pumpanen, J.; Sevanto, S.; Hari, P.; Nikinmaa, E.; Kaski, P.; Mannila, H.; Ukkonen, E.; et al. Autumn temperature and carbon balance of a boreal scots pine forest in southern Finland. *Biogeosciences* **2009**, *6*, 163–176. [CrossRef]
61. Suni, T.; Berninger, F.; Markkanen, T.; Keronen, P.; Rannik, Ü.; Vesala, T. Interannual variability and timing of growing-season CO_2 exchange in a boreal forest. *J. Geophys. Res. D* **2003**, *108*, 4265. [CrossRef]

62. Jung, M.; Reichstein, M.; Margolis, H.A.; Cescatti, A.; Richardson, A.D.; Arain, M.A.; Arneth, A.; Bernhofer, C.; Bonal, D.; Chen, J.; et al. Global patterns of land-atmosphere fluxes of carbon dioxide, latent heat, and sensible heat derived from eddy covariance, satellite, and meteorological observations. *J. Geophys. Res. D* **2011**, *116*, 245–255. [CrossRef]
63. Cleverly, J.; Eamus, D.; Coupe, N.R.; Chen, C.; Maes, W.; Li, L.; Faux, R.; Santini, N.S.; Rumman, R.; Yu, Q.; et al. Soil moisture controls on phenology and productivity in a semi-arid critical zone. *Sci. Total Environ.* **2016**, *568*, 1227–1237. [CrossRef] [PubMed]
64. Granath, G.; Strengbom, J.; Breeuwer, A.; Heijmans, M.M.; Berendse, F.; Rydin, H. Photosynthetic performance in Sphagnum transplanted along a latitudinal nitrogen deposition gradient. *Oecologia* **2009**, *159*, 705–715. [CrossRef] [PubMed]
65. Sun, F.; Kuang, Y.; Wen, D.; Xu, Z.; Li, J.; Zuo, W.; Hou, E. Long-term tree growth rate, water use efficiency, and tree ring nitrogen isotope composition of *Pinus massoniana* L. in response to global climate change and local nitrogen deposition in Southern China. *J. Soils Sediments* **2010**, *10*, 1453–1465. [CrossRef]
66. Norby, R.J.; Warren, J.M.; Iversen, C.M.; Medlyn, B.E.; McMurtrie, R.E. CO_2 enhancement of forest productivity constrained by limited nitrogen availability. *Proc. Natl. Acad. Sci. USA* **2010**, *107*, 19368–19373. [CrossRef] [PubMed]
67. Verma, M.; Friedl, M.A.; Richardson, A.D.; Kiely, G.; Cescatti, A.; Law, B.E.; Wohlfahrt, G.; Gielen, B.; Roupsard, O.; Moors, E.J.; et al. Remote sensing of annual terrestrial gross primary productivity from MODIS: An assessment using the FLUXNET La Thuile data set. *Biogeosciences* **2014**, *11*, 2185–2200. [CrossRef]